

Conformational Analysis, Molecular Modeling, and Quantitative Structure–Activity Relationship Studies of Agents for the Inhibition of Astrocytic Chloride Transport

Chris L. Waller,¹ Steven D. Wyrick,^{1,3}
W. Evans Kemp,¹ Hee Moon Park,¹ and
Forrest T. Smith²

Received August 1, 1992; accepted June 1, 1993

Molecular modeling studies were carried out on a series of 1-oxoisindolines which are pharmacologically active as inhibitors of astrocytic chloride transport. Conformational analysis revealed that the halogen substituent exerted a pronounced steric directing effect on the acid side chain. The 4-substituted analogs apparently provided for the best spatial arrangement of pharmacophoric elements of the molecules. Conventional quantitative structure-activity relationship (QSAR) studies using lipophilic and dipole moment characteristics of the molecules as physical descriptor variables in the regression equation yielded a statistically significant model. Comparative molecular field analysis (CoMFA) was utilized as a three-dimensional QSAR technique to explore changes in the steric and electrostatic fields of the molecules that can account for differences in biological activity values. A highly predictive model was attained which supported the results from the qualitative and conventional quantitative structure-activity relationship analyses. These modeling techniques represent the evolutionary process by which structure-activity methods were employed to aid in the development of novel more potent inhibitors of astrocytic chloride transport.

KEY WORDS: astrocytes; chloride; transport; quantitative structure-activity relationships (QSAR); comparative molecular field analysis; edema.

INTRODUCTION

Inhibitors of astrocytic chloride influx *in vitro* also prevent astrocytic swelling *in vitro* and *in vivo* (1–3). Compounds possessing this ability are potentially useful as therapeutic agents in the management of disorders associated with injury, such as cerebral edema (4,5) and stroke (6), as well as that associated with uric acid accumulation (7). We previously reported the biological activities of a series of 1-oxoisindolines with respect to inhibition of astrocytic chloride flux as measured in an *in vitro* assay using primary rat astrocyte cultures (8,9). The structural requirements necessary for the induction of biological activity for the 1-oxoisindolines have been examined by our group by structure-activity relationship studies, and based upon the de-

pendence of activity on finite regions or functionalities within the series, a preliminary pharmacophore has been developed. We propose the following: (1) the anionic acid functionality interacts with a complementary cationic site in the putative receptor binding domain; (2) the aromatic ring permits π - π stacking interactions; (3) the oxygen of the carbonyl acts as a hydrogen bond acceptor; and (4) the most distal carbon of the *N*-alkyl substituent indicates the extent of steric bulk tolerance in a hydrophobic binding pocket. Computer-assisted molecular modeling has been used to analyze the conformational differences between potent and relatively inactive inhibitors of astrocytic chloride influx and to provide information concerning the steric and electrostatic properties of the molecular binding domain of the receptor.

Others (7) have examined the structural requirements of a series of aryloxyalkanoic acids, compounds originally developed as astrocytic chloride transport inhibitors, which are necessary for the induction of uricosuric diuresis. These compounds are ring annealed derivatives of ethacrynic acid and structurally similar to the 1-oxoisindolines presented herein. Preliminary structure-activity relationship and receptor mapping studies of these compounds yielded a pharmacophore which exists in qualitative agreement with that proposed herein.

The ultimate goal of the present study was the development of a model in the form of a quantitative structure-activity relationship (QSAR) equation which could be used as a tool to aid in the development of novel, more potent inhibitors of astrocytic chloride transport. This was achieved by employing both conventional and state-of-the-art molecular modeling and statistical techniques.

MATERIALS AND METHODS

All of the molecular modeling techniques described herein were performed on either Evans and Sutherland ESV Workstations or a VAX 6330 mainframe computer using SYBYL 5.4 (10) molecular modeling software and MM2-87 (11) molecular mechanics software packages. The program StatView (12) was used to perform the conventional multiple regression analyses on Macintosh personal computers.

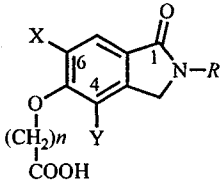
Molecular Modeling and Receptor Mapping Techniques. All molecules were graphically constructed *de novo* using the sketch option of the building component of the SYBYL 5.4 molecular modeling software package. Subsequently, the molecules were fully geometry optimized using the standard TRIPOS force field to an energy tolerance of 0.001 kcal/mol. All possible rotatable bonds located in the acid side chains and the nitrogen-alkyl junctions of the molecules were subjected to systematic conformational search routines. The bonds were rotated a full 360° at 10° increments. The lowest-energy conformer obtained from the search was once again optimized using the TRIPOS force field to allow for complete relaxation of the molecule.

The aforementioned pharmacophoric elements of the four most and four least active molecules 1, 2, 12, 14, 15, 16, 17, and 18, (Table I) including 4-chloro-, 6-chloro-, and nonchlorinated analogues, were connected by a spring force of 20 mdyne/Å. The eight molecule conglomerate was then minimized using the Multifit optimization routine in SYBYL

¹ Laboratory for Molecular Modeling, Division of Medicinal Chemistry and Natural Products, School of Pharmacy, University of North Carolina, Chapel Hill, North Carolina 27599-7360.

² Department of Pharmacal Sciences, School of Pharmacy, Auburn University, Auburn, Alabama 36849.

Table I. Structural and Biological Properties of Compounds Included in QSAR Analyses



No.	R	X	Y	n	pIC_{50} (M)
1	-CH ₃	Cl	H	3	1.78
2	-C ₂ H ₅	Cl	H	3	1.89
3	-C ₃ H ₇	Cl	H	3	2.56
4	-C ₄ H ₉	Cl	H	3	3.07
5	-c-C ₅ H ₉	Cl	H	3	2.20
6	-c-C ₆ H ₁₁	Cl	H	3	2.35
7	-c-C ₈ H ₁₅	Cl	H	3	3.23
8	-C ₂ H ₅	H	Cl	3	2.45
9	-C ₃ H ₇	H	Cl	3	2.87
10	-C ₄ H ₉	H	Cl	3	3.20
11	-c-C ₅ H ₉	H	Cl	3	2.94
12	-c-C ₆ H ₁₁	H	Cl	3	3.39
13	-c-C ₇ H ₁₃	H	Cl	3	3.11
14	-c-C ₈ H ₁₅	H	Cl	3	3.72
15	-2-CH ₃ -c-C ₆ H ₁₀ (e,e)	H	Cl	3	3.90
16	-Adamantyl	H	Cl	3	3.33
17	-CH ₃	H	H	3	2.25
18	-C ₂ H ₅	H	H	3	2.14

5.4. The total volume of the energy minimized structures was calculated using the MVolume option. Active volume contours were generated by subtracting the sum volume of representative structures from the relatively inactive series of molecules (1, 2, 17, and 18) from the total molecular volume. Inactive volume contours were calculated conversely.

Calculation of Dipole Moments Using MMP2(MM2-87) Algorithms and Development of a QSAR. The atomic coordinate files for the geometry optimized SYBYL 5.4 structures were converted from SYBYL 5.4 molecular file format to an input file readable by the MMP2(MM2-87) (11) program through the use of file conversion routines contained within the MODEL (13) molecular modeling software package. Once in MMP2 format, the structures were subjected to single-point energy calculations using a dielectric of 1.5 D. From these calculations, the dipole coordinates were obtained, along with a new coordinate file for the structure which included Cartesian coordinates for the molecule set relative to the MMP2-calculated center of mass. This file was then converted to SYBYL 5.4 molecular file format via the MMSYB software package developed in our laboratories (14) and transferred back into SYBYL 5.4 for visualization. Cartesian coordinates obtained for the dipole moment and the center of mass of the molecule were added to the molecular region as dummy atoms and a bond was drawn between these two points to graphically represent the dipole vector (Fig. 3).

The orientation of the resulting dipole vector was characterized using polar coordinates in the following manner. The length of the dipole vector is representative of the magnitude of the dipole moment and is reported herein (in Å) as

Table II. Root Mean Squares (RMS) Fit to the Template Molecule (15)^a

No.	C (acid)	Centroid	O (carbonyl)	C (alkyl)	RMS total
1	0.68	1.59	0.91	1.99	1.3940
2	0.91	1.67	0.85	1.64	1.3256
3	0.81	1.62	0.40	1.28	1.1275
4	0.63	0.34	0.55	0.69	0.5697
5	0.87	1.10	0.53	0.76	0.8405
6	0.92	0.98	0.54	0.81	0.8280
7	1.20	0.91	0.58	1.42	1.0749
8	0.29	0.77	0.87	1.58	0.9900
9	0.74	0.48	0.55	1.73	1.0106
10	0.03	0.07	0.07	0.07	0.0617
11	0.17	0.17	0.19	0.43	0.2651
12	0.04	0.05	0.07	0.05	0.0549
13	0.05	0.14	0.21	0.31	0.2004
14	0.22	0.27	0.30	0.78	0.4526
15	0.00	0.00	0.00	0.00	0.0000
16	0.05	0.06	0.14	0.09	0.0953
17	0.51	0.74	0.99	2.13	1.2570
18	0.34	0.80	0.88	1.58	1.0003

^a $pIC_{50} = 3.5200 - 1.0361$ (RMS total); $r = 0.810$; F test = 30.46; $P = 0.0001$.

ρ . To characterize further the dipole vector, a least-squares plane was constructed which contained the proposed four pharmacophoric elements of the molecule. A normal was then constructed to this "pharmacophoric plane" through the center of mass of the molecular. The angle of intersection between the dipole vector and this normal is termed θ herein. To describe the rotation of the dipole vector about the normal relative to a reference point, two least-squares planes were generated. The first plane contained the dummy atom representing the dipole moment, the center of mass of the molecule, and one of the two dummy atoms used to define the bond describing the normal. The second plane, or reference plane, contained these same points with the exception that the dipole moment dummy atom was replaced by the sp^2 oxygen of the carbonyl. The orientation of the dipole rotation about the normal was then determined by calculating the angle between these two planes and labeled ϕ . In Fig. 3, molecule 15 is shown with the associated dipole moment vector and planes.

Calculated n -octanol:water partition coefficients, or $\log P$ values, were determined through the use of a computational method contained within the Pomona Medchem Database (15) and, along with ρ and cosine θ , served as regressor variables in the conventional QSAR equations.

COMPARATIVE MOLECULAR FIELD ANALYSIS (CoMFA) QSAR METHODOLOGIES

Alignment Rules. The ionized forms of the lowest-

Table III. Covariance Between Bioactivity Values (pIC_{50}) and Total RMS Deviation Between Pharmacophoric Elements

C (acid)	Centroid	O (carbonyl)	C (alkyl)	Total
-0.13	-0.289	-0.166	-0.329	-0.244

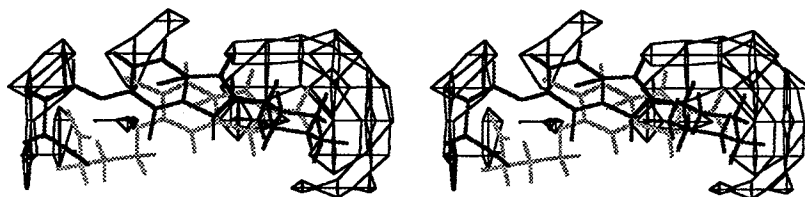


Fig. 1. Stereoview (crossed) of the active volume contour map. The active molecule (15) is black. The inactive molecule (1) is gray.

energy conformations determined by SYBYL 5.4 with charges calculated by the method of Del Re were used in all of the following analyses. Four methods of molecular alignment were examined in this comparative study. All molecules were aligned relative to compound 15, the most active analogue, using variations of the root mean squares (RMS) fit routine or the field-fit minimization option in SYBYL 5.4. The first two alignments were generated using RMS fit routines. Alignment I was the RMS fit of the 1, 4, and 6 carbons of the 1-oxoisindoline core of the molecules. Alignment II was the RMS fit of the pharmacophoric elements of the molecules. Alignment III, a variation of the field-fit option, allowed the bond distances, bond angles, and torsion angles of the test molecules to be altered during the procedure while holding the template molecule rigid in order to maximize the overlap between the electronic and the steric fields of the template and the test molecule at the expense of structural potential energy increases. Alignment IV provided for a subsequent non-field-fit reoptimization of the high-energy structures which resulted from the previous alignment rule. This final optimization using the standard TRIPOS force field allowed the molecules to relax to the nearest local energy minimum conformation.

CoMFA Interaction Energy Calculations. The steric, in terms of the van der Waal's (6–12) interactions, and electrostatic, coulombic with a $1/r$ distance-dependent dielectric function, potential energy fields were calculated at each lattice intersection on a regularly spaced grid. The grid spacing was 2.0 Å in each direction, with the grid extending 4.0 Å in every direction away from molecule. An sp^3 carbon probe atom with a van der Waal's radius of 1.52 Å and a +1.0 charge was used in the calculations.

Statistical Methods. The initial analysis, in all cases, was performed using the partial least squares (PLS) (16,17) algorithm in conjunction with the cross-validation option. One cross-validation (16) group was used per observation so that each compound would be systematically excluded from the analysis. The initial number of components was set to five. Following this analysis, assuming that an acceptable cross-validated r^2 (generally greater than 0.5) and a reason-

able number of components were obtained, a second PLS analysis was performed using the optimum number of components and no cross-validation. This second analysis allowed for graphical representation of the results as contour plots. A third analysis, which included 10 bootstrap (16) groups, was then performed to obtain confidence limits. Numerical statistical results for all of the analyses are listed in Table VI.

RESULTS AND DISCUSSION

Conformational Analysis. The compounds listed in Table I were constructed, geometry optimized, and conformationally searched using SYBYL 5.4 (10) algorithms (see Materials and Methods). Upon visual inspection of the geometry of the energy-minimized structures, it is obvious that the presence and relative position of the halogen on the aromatic ring exert the predominant steric directing effect on the acid side chain of the molecules. The orientation of the *N*-alkyl substituent is unaffected by, and likewise does not influence, the orientation of the butyric acid side chain. Therefore, within the individual 4-chloro, 6-chloro, and nonchlorinated series of molecules, the torsion angles of the acid side chain remain relatively constant.

RMS Fit of Pharmacophoric Elements. The utilization of this technique presupposes the applicability of a pharmacophore hypothesis. The hypothesis as currently viewed states the existence of four pharmacophoric elements in the molecules of interest. These elements are those atoms or functional groups that have been determined *via conventional structure-activity techniques* to be essential for the expression of biological activity. For the molecules presented herein, these elements are as follows: (i) the terminal, or most distal, alkyl atom of the *R* substituent; (ii) the sp^2 oxygen of the carbonyl; (iii) the centroid of the aromatic ring; and (iv) the sp^2 carbon of the acid moiety of the side chain since there is little energy barrier to rotation of the carboxyl group itself.

The 4-chloro-*N*-2-methylcyclohexyl derivative (15) and the 4-chloro-*N*-cyclooctyl derivative (14) proved to be the

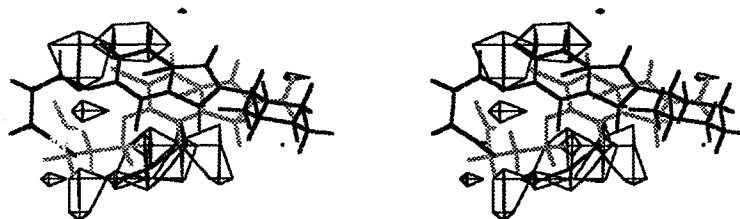


Fig. 2. Stereoview (crossed) of the inactive volume contour map. The active molecule (15) is black. The inactive molecule (1) is gray.

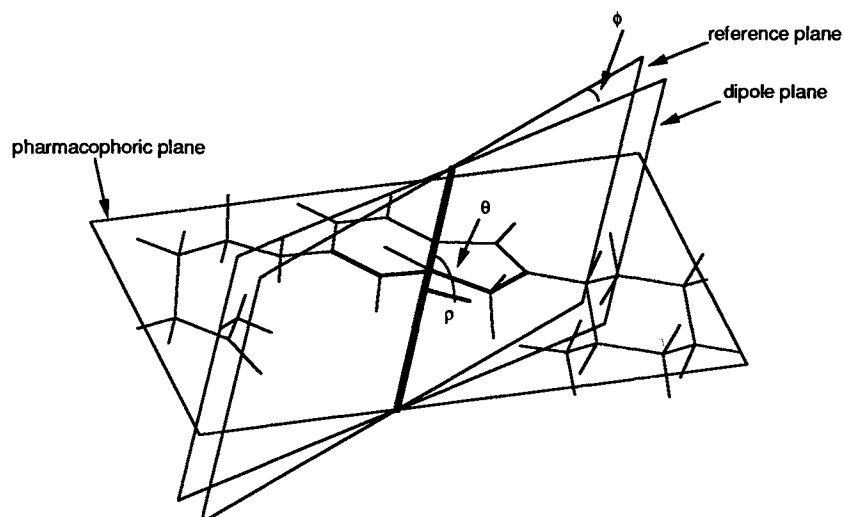


Fig. 3. Dipole moment vector characterization.

best inhibitors of *in vitro* rat astrocytic chloride transport (8). Therefore, it was concluded that these molecules present the optimal spatial arrangement of pharmacophoric elements to the putative receptor. For this reason, the slightly more active compound 15 was chosen as the template molecule to which all others were to be compared by the RMS fitting routine in SYBYL 5.4. Table II contains the RMS distance values (Å) between the pharmacophoric elements of the template (15) and test molecules.

A least-squares analysis of the total RMS deviation and biological activity values yielded a correlation coefficient (r) of 0.810. It is evident from the degree of covariance (-0.329) noted between the terminal alkyl pharmacophoric atom and the biological activity values (Table III) that the putative receptor appears to exhibit a large degree of steric bulk tolerance in the area of the *N*-alkyl substituents.

Multifit Analysis: Receptor Mapping. The Active Analogue Approach (18) has historically proven to be quite useful in obtaining information regarding the physical properties

of receptors in the absence of experimental data (i.e., X-ray crystallographic or NMR data). As employed herein, this method is a modification of the RMS fit technique and is also dependent on the pharmacophore hypothesis stated above.

The proposed pharmacophoric elements of a subseries of our compounds which included both active and relatively inactive analogues were linked by a spring force, and the entire conglomerate was then minimized using the Multifit optimization routine of SYBYL 5.4. Molecular volume contour maps were used to analyze the results of the analysis and to designate areas in space, presumably associated with the molecular binding domain of the putative receptor, which either contribute to or detract from biological activity. In Fig. 1, the contours represent the active volume of the molecular binding domain. A large degree of concentrated steric bulk appears to be tolerated in the area of the alkyl substituent. It is also suggested that the orientation of the acid side chain is a contributing factor to bioactivity. Analogues chlorinated in the 4-position are consistently more active than their corresponding 6-chloro or nonchlorinated derivatives and the orientation of the side chain is clearly different among the three types of compounds. Presumably, the 4-chloro derivatives direct the side chain in a direction such as to occupy necessary receptor space, whereas the acid side chains of the 6-chloro and nonchlorinated analogs extend

Table IV. Dipole Vector Orientation and Lipophilicity Values

No.	$\cos\theta$	$\cos\phi$	ρ (Å)	$c \log P$
1	-0.196	0.333	6.551	0.842
2	0.214	0.394	6.536	1.371
3	0.432	0.468	6.437	1.900
4	-0.224	0.641	4.245	2.429
5	-0.345	0.484	6.644	2.224
6	-0.476	0.531	6.487	2.783
7	0.424	0.515	6.621	3.901
8	-0.647	0.991	4.196	1.371
9	-0.317	0.489	4.184	1.900
10	-0.640	0.999	2.665	2.429
11	-0.568	0.855	4.228	2.224
12	-0.632	0.994	2.625	2.783
13	-0.597	0.994	2.464	3.342
14	-0.613	0.973	2.503	3.901
15	-0.608	0.990	2.489	3.302
16	-0.568	1.000	2.657	3.411
17	-0.493	0.879	3.888	0.324
18	-0.292	0.841	3.932	0.853

Table V. Conventional QSAR Results

Regressor(s)	r^2	SE	F test	P value
$c \log P$	0.662	0.373	31.289	0.0001
ρ	0.491	0.457	15.448	0.0012
$\cos\theta$	0.125	0.599	2.283	0.1503
$\cos\phi$	0.469	0.467	14.134	0.0017
$c \log P$ (ρ)	0.882	0.228	55.868	0.0001
$c \log P \cos\theta$	0.730	0.344	20.265	0.0001
$c \log P \cos\phi$	0.856	0.251	44.488	0.0001
$\rho, \cos\theta$	0.552	0.443	9.248	0.0024
$\rho, \cos\phi$	0.499	0.468	7.482	0.0056
$c \log P, \rho, \cos\phi$	0.900	0.217	41.849	0.0001
$c \log P, \rho, \cos\phi$	0.882	0.235	34.916	0.0001

	ρ	$c \log P$	$\cos \theta$	$\cos \phi$
ρ	1			
$c \log P$	-0.314	1		
$\cos \theta$	0.741	-0.116	1	
$\cos \phi$	-0.93	0.331	-0.725	1

Fig. 4. Correlation matrix for physical descriptor variables used in conventional QSAR studies.

into areas of low bulk tolerance (inactive volumes) lacking the cationic binding site (Fig. 2). Although the results of the Active Analogue Approach are highly informative, it must be cautioned that this technique is highly qualitative and the predictive ability is limited.

Dipole Moment Characterization and the Development of a QSAR. The use of molecular mechanical dipole moment characteristics as molecular electronic descriptors of biological activity is well represented in the literature (19–21). In the present work, the dipole moment was described relative to a least-squares plane which contained the pharmacophoric elements of the molecule (Fig. 3). This method efficiently combined electronic (dipole moment vector) and steric (pharmacophoric elements described by a plane) elements into one regressor variable. The cosine of the angle between the dipole vector and the normal constructed to the pharmacophoric plane through the center of mass of the molecule, $\cos\theta$, as well as the rotation of the dipole vector about the normal expressed relative to a common reference plane, $\cos\phi$, were used as physical descriptors of biological activity (Fig. 3). The length, ρ , of the dipole vector (\AA) provided for a measure of the magnitude of the electronic effect and proved to be a useful regressor variable. The calculated lipophilicity values (15), $c \log P$, of the molecule were used to quantitatively represent the steric bulk tolerance of hydrophobic groups noted in the RMS fit and pharmacophore mapping studies. This physical descriptor served a twofold purpose, as it also provided an indication of the transportability of the molecule across or into biological membranes. All of the above values are given in Table IV.

Although $\cos\theta$ and $\cos\phi$ alone were not particularly strong physical descriptors ($r^2 = 0.125$ and $r^2 = 0.469$, respectively), when used in combination with the other regressors, they consistently increased the correlative values of bivariate analyses (Table V). As regressors in trivariate analyses, $\cos\theta$ and $\cos\phi$ either affected only minimally or did not significantly alter the significance of the correlations ($r^2 = 0.900$ and $r^2 = 0.882$, respectively) with respect to the corresponding bivariate analysis ($r^2 = 0.882$ with $c \log P$ and ρ as regressors). With 18 observations (compounds), the use of

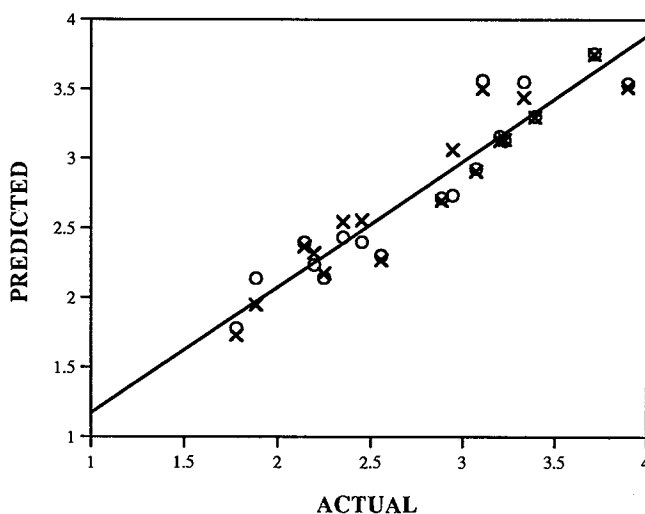


Fig. 5 Overlay plot of actual versus predicted biological activity values calculated from conventional (X) and CoMFA (O) QSAR equations.

not more than three regressor variables was recommended in order to limit the occurrence of spurious correlations within the dataset (22). Upon examination of the correlation matrix (Fig. 4) for all four regressor variables, a significant cross-correlation was noted between ρ and $\cos\phi$. Considerable cross-correlations also existed between $\cos\theta$ and both $\cos\phi$ and ρ ; therefore, it was decided that two of these regressors ($\cos\theta$ and $\cos\phi$) should be excluded. The resulting bivariate regression analysis produced the best model ($r^2 = 0.882$ using only two regressors), with a standard error (0.228) comparable to that of the trivariate models representing a simple correlation between activity and two scalar properties. The β coefficients associated with each regressor variable and y intercept were also calculated and used to generate the following QSAR equation:

$$pIC_{50} = 2.71 - 0.18\rho + 0.39 \log P$$

$$(n = 18, SE = 0.228, F = 55.835, P = 0.0001) \quad (1)$$

The relationship between these variables and the geometric orientation of the chosen pharmacophore may not be immediately obvious; however, this correlation represents a model which may have potential as a tool to aid in the design of novel, more potent chloride flux inhibitors. Equation (1) was used to predict the biological activities of the molecules included in the analysis, and these values are shown plotted versus the actual values in Fig. 5.

Table VI. CoMFA QSAR Results

Alignment	r^2_{cross}	r^2	SE	F test	r^2_{bs}	SD
I	0.817 (3)	0.930 (3)	0.181	62.372	0.950	0.025
II	0.814 (2)	0.901 (2)	0.208	68.118	0.911	0.040
III	0.783 (2)	0.892 (2)	0.217	61.993	0.916	0.028
IV	0.821 (2)	0.906 (2)	0.203	72.042	0.913	0.038

^a Values in parentheses are optimal numbers of components. P values for all analyses = 0.000.

Alignment rules: I, RMS fit of core atoms; II, RMS fit of pharmacophoric atoms; III, field-fit optimization; IV, field-fit optimization with subsequent reoptimization.

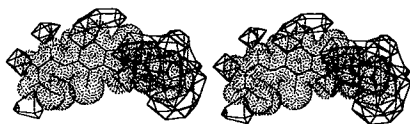


Fig. 6. Stereoview (crossed) of the positive steric contribution contour plot. $SD \cdot Coefficient = 0.006$ kcal/mol. The molecule is 15.

CoMFA as a QSAR Tool. The numerical results of several CoMFA (23–25) analyses are found in Table VI. Each of the analyses represents one particular alignment of the 4-chloro, 6-chloro, and nonchlorinated analogues within the QSAR database. Due to the regressor-heavy nature of a CoMFA QSAR table, multiple regression is both computationally and statistically inappropriate. Therefore, a type of principal components analysis, namely, partial least squares (PLS) (16), was utilized in conjunction with cross-validation (16) to examine the table in a computationally efficient manner and minimize the occurrence of spurious correlations. The “best” analysis was defined as the one requiring the least number of principal components in order to achieve the highest cross-validated r^2 value. The bootstrap (16) technique was utilized to provide a means by which statistical confidence limits could be placed on the analyses.

Four particular methods of molecular alignment were examined in this study. Two were variations of RMS fit procedures of selected atoms, while the others resulted from field-fit analyses performed on the molecules. Alignment rule I was selected in order to maximize the superimposition of the 1-oxoisindoline substructure shared by all of the molecules while allowing the structural variability to be represented by the orientations and sizes of the acid side chains and the *N*-alkyl substituents. This alignment yielded promising cross-validated results, but the highest probability of spurious correlations, as represented by the difference between cross-validated and non-cross-validated r^2 values, was noted. An RMS fit of the pharmacophoric elements was chosen as alignment rule II as a logical extension of the RMS fit analyses presented above. Once again, the choice of pharmacophoric atoms was supported in that this alignment produced acceptable cross-validated and non-cross-validated results. The optimal number of components as well as the chance of spurious correlations was lessened using this alignment rule.

The first alignment rule, which utilized the field-fit option, alignment III, allowed the conformations of the test compounds to be altered, at the expense of potential energy, in order to maximize the steric and electrostatic field overlap between template 15 and test molecules. The analysis based on this alignment yielded weaker yet statistically acceptable results. When the energetically and geometrically unrealistic conformations generated by the above method were allowed to return to the nearest local energy minimum conformation

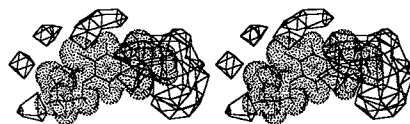


Fig. 7. Stereoview (crossed) of the positive steric contribution contour plot. $SD \cdot Coefficient = 0.006$ kcal/mol. The molecule is 1.



Fig. 8. Stereoview (crossed) of the negative steric contribution contour plot. $SD \cdot Coefficient = -0.006$ kcal/mol. The molecule is 15.

(reoptimized), as was the case with alignment IV, a highly predictive ($r^2_{cross} = 0.821$) and statistically valid ($r^2 = 0.906$, F test = 72.042) model was attained.

In Fig. 5, the predicted biological activity values obtained from the CoMFA study based on alignment rule IV are shown plotted versus the actual values. These results are visually comparable to those from the conventional QSAR studies also plotted in Fig. 5. Since each column in the CoMFA table corresponds directly to a specific point on the lattice in the region surrounding the molecules, various factors of the resultant QSAR equations can be extracted and graphically plotted versus molecular structural characteristics. This functionality provides CoMFA with an incomparable advantage over the more conventional QSAR techniques. In Figs. 6 and 7, the contours, generated by an extrapolation technique, encompass lattice points where the scalar products of the β coefficient and the standard deviation associated with a particular steric column (lattice intersection) in the data table were a user-defined positive value of 0.006. In these areas, increases in biological activity were noted with increases in steric bulk. It can be seen that the van der Waal's volume of the most active molecule, 15 (template), represented as a dot surface, almost completely fills the required areas (Fig. 6), while the volume of the inactive molecule, 1, does not (Fig. 7). The converse situation is plotted in Figs. 8 and 9 in that the contours designate areas in space where increases in steric bulk are associated with decreased bioactivity. The volume of the inactive molecule extends into the sterically detrimental areas (Fig. 8), while the active molecule's volume does not (Fig. 9). These positive and negative steric contours correlate well with the active and inactive volumes (Figs. 1 and 2) which results from the multifit analysis.

In conclusion, conventional QSAR and CoMFA studies gave similar results. Both techniques correlate biological activity with the steric and electronic character of the analogues, while the conventional QSAR also employs lipophilicity as a descriptor. This molecular characteristic may also be inherent in the CoMFA studies since correlations have been found between lipophilicity and steric and electrostatic fields for molecules.

The most promising (26–30) of the methods presented herein is CoMFA. Drug–receptor interactions are predominantly noncovalent and are manifested primarily as functions of the shapes and charge distributions associated with both the receptor and the ligand molecule. The CoMFA al-

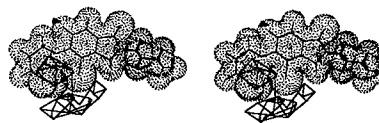


Fig. 9. Stereoview (crossed) of the negative steric contribution contour plot. $SD \cdot Coefficient = -0.006$ kcal/mol. The molecule is 1.

gorithms were developed with this in mind and provide for a full description of the steric and electrostatic properties of the ligand molecules. Pharmaceutically useful facets of CoMFA include statistical data management, i.e., the cross-validation process, and the ability to produce plots which can be used as guides during the drug design process. While other, more conventional, QSAR methods attempt to predict (extrapolate) new target properties (biological activities) based on correlations drawn between existing biological data and partially descriptive regressor variables, predictability exists as the heart of the CoMFA technique.

ACKNOWLEDGMENTS

The authors wish to thank TRIPOS Associates for their generous support in supplying the SYBYL 5.4 software to the Laboratory for Molecular Modeling, Division of Medicinal Chemistry and Natural Products, School of Pharmacy, University of North Carolina at Chapel Hill, and Dr. Richard Cramer for valuable assistance with CoMFA.

REFERENCES

1. E. J. Cragoe, N. P. Gould, O. W. Woltersdorf, C. Ziegler, R. S. Bourke, L. R. Nelson, H. K. Kimelberg, J. B. Waldman, A. J. Popp, and N. Sedransk. Agents for the treatment of brain injury. 1. (Aryloxy)alkanoic acids. *J. Med. Chem.* 25:567-579 (1982).
2. H. K. Kimelberg and M. V. Frangakis. Furosemide- and bumetanide-sensitive ion transport and volume control in primary astrocyte cultures from rat brain. *Brain Res.* 361:125-134 (1985).
3. H. K. Kimelberg, J. W. Rose, K. D. Barron, R. A. Waniewski, and E. J. Cragoe. Astrocytic swelling in traumatic-hypoxic brain injury: Beneficial effects of an inhibitor of anion exchange transport and glutamate uptake in glial cells. *Mol. Chem. Neuropathol.* 11(1):1-31 (1989).
4. D. P. Becker, D. J. Miller, J. D. Ward, R. P. Greenberg, H. F. Young, and R. Sakalas. The outcome from severe head injury with early diagnosis and intensive management. *J. Neurosurg.* 47:491-502 (1977).
5. L. F. Marshall, R. W. Smith, and H. M. Shapiro. The outcome with aggressive treatment in severe head injuries. II. Acute and chronic barbiturate administration in the management of head injury. *J. Neurosurg.* 50:26-30 (1979).
6. B. K. Siesjo. Cerebral circulation and metabolism. *J. Neurosurg.* 60:883-908 (1984).
7. H. Koga, H. Sato, T. Dan, and B. Aoki. Studies on uricosuric diuretics. 4. Three-dimensional structure-activity relationships and receptor mapping of (aryloxy)acetic acid diuretics. *J. Med. Chem.* 34:2702-2708 (1991).
8. C. L. Waller, S. D. Wyrick, H. M. Park, W. E. Kemp, and F. T. Smith. Effects of [(N-alkyl-1-oxo-1H,3H-isoindolin-5-yl)oxy]alkanoic acids on chloride transport in primary astroglial cultures. *J. Pharm. Sci.* (in press).
9. S. D. Wyrick, F. T. Smith, W. E. Kemp, and A. A. Grippo. Effects of [(N-alkyl-1,3-dioxo-1H,3H-isoindolin-5-yl)oxy]alkanoic acids, [(N-alkyl-1-oxo-1H,3H-isoindolin-5-yl)oxy]butanoic acids, and related derivatives on chloride influx in primary astroglial cultures. *J. Med. Chem.* 30:1798-1806 (1987).
10. SYBYL 5.4, TRIPOS Associates, St. Louis, MO (1991).
11. N. Allinger *et al.* MMP2(MM2-87) software, Molecular Design, Ltd.
12. StatView 512+ software package, Brain Power, Inc., Calabasas, CA (1986).
13. C. Still and K. Steliou *et al.* MODEL, Version 2.91, K, Quebec, Canada.
14. A. J. Hoffman and P. S. Charifson. MMSYB software (unreleased) (1988).
15. A. Leo, C. Hansch, and D. Elkins. Partition coefficients and their uses. *Chem. Rev.* 71:525-616 (1971).
16. R. D. Cramer, J. D. Bunce, D. E. Patterson, and I. E. Frank. Crossvalidation, bootstrapping, and partial least squares compared with multiple regression in conventional QSAR studies. *Quant. Struct.-Act. Relat.* 7:18-25 (1988).
17. S. Wold, A. Ruhe, H. Wold, and W. J. Dunn. The covariance problem in linear regression. The partial least squares (PLS) approach to generalized inverses. *SIAM J. Sci. Stat. Comp.* 5(3):735-743 (1984).
18. G. R. Marshall. Structure-activity studies: A three-dimensional probe of receptor specificity in macromolecular structure and specificity: Computer-assisted modeling and applications. *Ann. N.Y. Acad. Sci.* 439:162-169 (1985).
19. P. S. Charifson, J. P. Bowen, S. D. Wyrick, A. J. Hoffman, M. Cory, A. T. McPhail, and R. B. Mailman. Conformational analysis and molecular modeling of 1-phenyl, 4-phenyl, and 1-benzyl-1,2,3,4-tetrahydroisoquinolines as D₁ dopamine receptor ligands. *J. Med. Chem.* 32:050-2058 (1989).
20. R. C. Young, G. J. Durant, J. C. Emmett, C. R. Ganellin, M. J. Graham, R. C. Mitchell, H. D. Prain, and M. L. Roantree. Dipole moment in relation to H₂ receptor histamine antagonist activity for cimetidine analogs. *J. Med. Chem.* 29:41-49 (1986).
21. Y. Inami, T. Tomita, and Y. Terada. Quantitative structure-activity relationship analysis of phencyclidine derivatives. *I. Chem. Pharm. Bull.* 39(6):1426-1429 (1991).
22. J. G. Topliss, and R. P. Edwards. Chance factors in QSAR studies. In E. C. Olson and R. E. Christofferson (eds.), *Computer-Assisted Drug Design, ACS Symposium Series 112*, American Chemical Society, Washington, DC, 1979, pp. 131-145.
23. R. D. Cramer and J. D. Bunce. The dylomms method: Initial results from a comparative study of approaches to 3D QSAR. In D. Hadzi and B. Jerman-Blazic (eds.), *QSAR in Drug Design and Toxicology*, Elsevier Science, Amsterdam, 1987, pp. 3-12.
24. R. D. Cramer, D. E. Patterson, and J. D. Bunce. Comparative molecular field analysis (CoMFA). 1. Effect of shape on binding of steroids to carrier proteins. *J. Am. Chem. Soc.* 110:5959-5967 (1988).
25. R. D. Cramer, D. E. Patterson, and J. D. Bunce. Recent advances in comparative molecular field analysis (CoMFA). In J.-L. Fauchere (ed.), *QSAR: Quantitative Structure-Activity Relationships in Drug Design*, Alan R. Liss, New York, 1989, pp. 161-165.
26. K. H. Kim and Y. C. Martin. Direct prediction of dissociation constants (pK_a's) of clonidine-like imidazolines, 2-substituted imidazoles, and 1-methyl-2-substituted-imidazoles from 3D structure using a comparative molecular field analysis (CoMFA) approach. *J. Med. Chem.* 34:2056-2060 (1991).
27. F. I. Carroll, Y. Gao, M. A. Rahman, P. Abraham, K. Parham, A. H. Lewin, J. W. Boja, and M. J. Kuhar. Synthesis, ligand binding, QSAR, and CoMFA study of 3β-(p-substituted phenyl) tropane-2β-carboxylic acid methyl esters. *J. Med. Chem.* 34:2719-2725 (1991).
28. J.-P. Bjorkroth, T. A., Pakkanen, J. Lindroos, E. Pohjala, H. Hanhijarvi, L. Lauren, R. Hannuniemi, A. Juhakoski, K. Kippo, and T. Kleimola. Comparative molecular field analysis of some clodronic acid esters. *J. Med. Chem.* 34:2338-2343 (1991).
29. B. F. Thomas, D. R. Compton, B. R. Martin, and S. F. Semus. Modeling the cannabinoid receptor: A three-dimensional quantitative structure-activity analysis. *Mol. Pharmacol.* 40:656-665 (1991).
30. C. L. Waller and J. D. McKinney. Comparative molecular field analysis of polyhalogenated dibenzo-p-dioxins, dibenzofurans, and biphenyls. *J. Med. Chem.* (1992).